EXHIBIT F

Charge-transfer-plate spatial light modulators

Cardinal Warde, Craig M. Schiller, Jeffrey Bounds, Thomas N. Horsky, George Melnik, and Robert Dillon

Charge-transfer-plate spatial light modulators (CTPSLM's) are a class of devices that employ charge-transfer plates as the interface between the charge-generation element and the light-modulation element. Both optically addressed and electrically addressed devices have been built. Charge-generating elements for the optically addressed devices include photoconductors, photodiode and phototransistor arrays, optoelectronic integrated circuit chips, and photocathode–microchannel-plate assemblies. For electrically addressed devices, electron guns, very large-scale integrated circuits, thin-film transistors, and matrix electrodes are among the possible charge-generation elements. Light-modulation elements used in CTPSLM's include liquid crystals, electro-optic organic and inorganic crystals, polymers, deformable membrane mirrors, oil films, multilayer dielectric films, and electroluminescent films. In principle, all combinations of charge-generation elements and light-modulating elements are possible. This paper explores the fundamental performance limitations of CTP technology, and describes the design, operation, and applications of five different CTPSLM's (three based on membrane-mirror technology and two on liquid-crystal technology).

1. Introduction

Two-dimensional spatial light modulators (SLM's) are the building blocks of optical information processors.[1] SLM's modify the amplitude, phase, polarization, or intensity of a readout light beam in response to either the intensity of a second write-light beam or to a two-dimensional electrical voltage or current pattern. Devices of the first type are called optically addressed SLM's and devices of the second type are called electrically addressed SLM's, respectively.

Charge-transfer-plate spatial light modulators (CTPSLM's) are a relatively new class of devices that employ the structure shown in Fig. 1, in which a charge-transfer plate (CTP) is used as the interface between the charge-generation element and the light-modulation element. The general CTPSLM may also contain an optional gain element, as shown in Fig. 1.

When the work was performed the authors were with Optron Systems, Inc., 3 Preston Court, Bedford, Massachusetts 01730. C. Warde's permanent address is the Department of Electrical Engineering and Computer Science, Massachusetts Institute of Technology, Cambridge, Massachusetts 02139. J. Bounds is now with the Department of Electrical Engineering and Computer Science, Massachusetts Institute of Technology, Cambridge, Massachusetts 02139. R. Dillon is presently with Sparta, Inc., 24 Hartwell Avenue, Lexington, Massachusetts 02173.

Received 28 August 1991.
0003-6935/92/203971-09$05.00/0.

As illustrated in Fig. 2, a CTP is essentially a dense array of longitudinally oriented conducting pins embedded in a wafer of electrically insulating material. The CTP derives its name from its ability to serve as a high-density multifeedthrough vacuum interface that can transfer a two-dimensional charge distribution from vacuum to air. CTP's that are 25 mm in diameter with 50-μm-diameter conducting pins on 70-μm centers, and with 10-μm-diameter conductors on 14-μm centers in hexagonal close-packed patterns, have been built in thicknesses up to 5 mm. Thus the ratio of a collective pin cross-sectional area to the total CTP area is ~50%. The surfaces of the CTP can be highly polished to an optical flatness of $\lambda/10$.

Charge-generating elements for the optically addressed CTPSLM's include photoconductors, photodiode and phototransistor arrays, optoelectronic integrated circuit chips, and photochathode–microchannel-plate (MCP) assemblies. On the other hand, electron guns, very large-scale integrated (VLSI) circuits, thin-film-transistors, and matrix electrodes are among the possible charge-generation elements for electrically addressed devices. Light-modulation elements that can be used in CTPSLM's include liquid crystals, electro-optic organic and inorganic crystals, polymers, deformable membrane mirrors, oil films, multilayer dielectric films, and electroluminescent films. In principle, all combinations of charge-generation elements and light-modulating elements are possible.

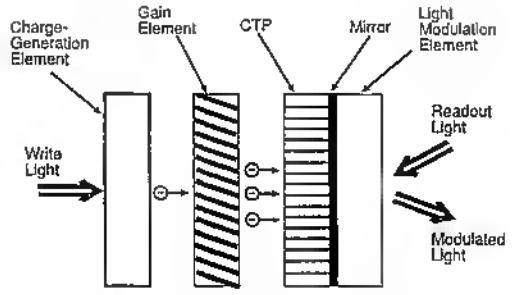

Fig. 1. Architecture of CTPSLM's.

This paper describes the characteristics of CTP's and structure, principles of operation, and applications of five different CTPSLM's (three based on membrane-mirror technology and two based on liquid-crystal technology).

2. CTP Characteristics

A. CTP-Limited Spatial Resolution

The spatial resolution of a light modulator with the architecture shown in Fig. 1 may be limited by the spatial rsolution of any of its constituents (the charge generation, gain, CTP, or light-modulation element). We are concerned here with only the influence of the CTP on the resolution of the SLM.

The spatial resolution of the CTP is determined primarily by CTP thickness, interpin separation, pin diameter, pin array pattern, and the CTP insulator material resistivity and dielectric constant. These parameters detemine the interpin capacitance and resistance, and therefore the extent to which a charge placed on one pin raises the voltage on that pin as well as on the neighboring pins. The spatial resolution of the CTP has been studied by electrostatic modeling techniques and confirmed by experiments involving the transfer of voltage longitudinally through the CTP to thin liquid-crystal layers.

In the electrostatic model, only two dimensions were considered, so that fringing effects at the face of the plate were neglected. The fringing effects should be negligible, considering the pin geometry. By treating the CTP charge-to-voltage response with a linear-systems analysis, we may use a spatial point-spread function representation to characterize the spatial resolution of the CTP. Thus the voltage on any pin can be determined from a superposition of all contributions arising from charge on the other pins plus the component, because of the self-capacitance of the pin itself.

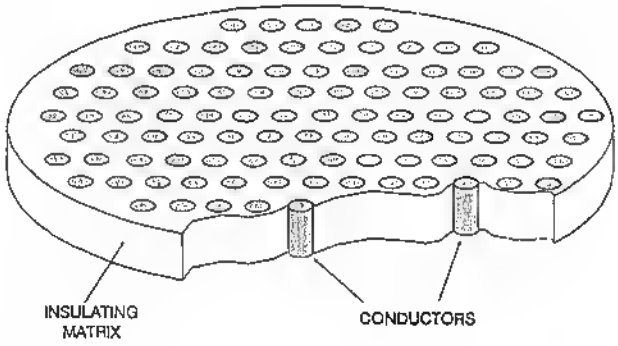

Fig. 2. CTP is a close-packed array of conductors embedded in an insulating matrix.

The generalized distributed capacitance problem can be modeled by the equation

$$\mathbf{V} = \mathscr{C}^{-1}\mathbf{q}, \tag{1}$$

where $\mathbf{q}$ and $\mathbf{V}$ are vectors representing the charge and voltage respectively on each pin, and $\mathscr{C}^{-1}$ is the inverted capacitance matrix. Alternatively, we may write

$$\begin{bmatrix} q_1 \\ \vdots \\ q_n \end{bmatrix} = \begin{bmatrix} C_{11} & \cdots & C_{1n} \\ \vdots & & \vdots \\ C_{n1} & \cdots & C_{nn} \end{bmatrix} \begin{bmatrix} V_1 \\ \vdots \\ V_n \end{bmatrix}. \tag{2}$$

Because the CTP pins are hexagonally packed, we need only solve for fields in one-sixth of the plate. Thus we determined the capacitance matrix by using a two-dimensional finite-difference numeric field approximation that solved Poisson's equation with a relaxation technique over an equilateral triangular mesh. The main difficulty with this technique, aside from the length of computation time, was the bookkeeping involved in translating from the triangular mesh to the inherent Cartesian coordinate structure of a matrix.

The procedure for calculating the capacitance matrix was as follows. One pin was assigned a potential with respect to a reference (ground) at infinity, and the relaxation method was used to solve for charge distributions resulting from the imposed potential. We supplied the algorithm with a series of unit test voltage vectors ($\mathbf{V}_1$ to $\mathbf{V}_n$) to obtain approximations to each column of the capacitance matrix. For example,

$$\mathbf{V}_1 = \begin{bmatrix} 1 \\ 0 \\ \vdots \\ 0 \end{bmatrix} \Rightarrow \mathbf{q}(\mathbf{V}_1) = \begin{bmatrix} C_{11} \\ \vdots \\ C_{n1} \end{bmatrix}. \tag{3}$$

Thus we obtained the $\mathscr{C}$ matrix, which, when inverted, allowed us to compute the voltage distribution developed on the pins in response to an applied charge distribution. Specifically, by applying charge to only one pin, we found the spatial point-spread function, which is illustrated in Fig. 3, from the model. The lower part of Fig. 3 shows the voltages on the charged pin (pin 0) and two adjacent uncharged pins (pin 1 and pin 2) on a sectional cut along the x axis. From

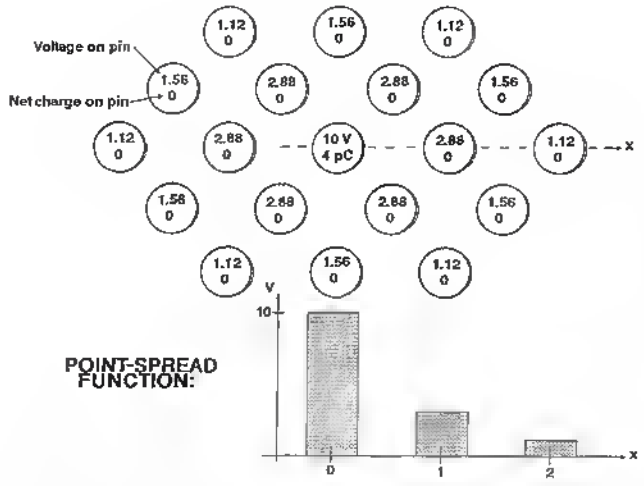

Fig. 3. Calculated normalized pin voltages that are due to capacitance coupling for a hexagonally packed CTP in response to a charge q placed on one pin.

Fig. 3 we see that if V is the voltage developed on a CTP pin in response to a charge q placed on that pin, the voltage developed on the neighboring pins is of the order of $V/3$, and $\sim V/10$ on the next-nearest-neighbor pins. Note also that for a 4-mm-thick CTP with 50-μm conducting pins on 70-μm centers the CTP pin self-capacitance is found to be approximately 0.4 pF.

In practice, CTP's may exhibit fixed-pattern noise arising from irregularities in the packing of the pins, and these irregularities may be evident in the modulated output image. This would be true especially in systems that do not spatially filter the diffraction pattern from the modulator before reimaging to form the output image. A liquid-crystal CTPSLM that is read out between crossed polarizers is an example. Of course, the ideal system is one in which the CTP resolution is at least a factor of 2 higher than that of the element with the next-highest resolution.

B. Secondary Electron Emission Characteristics of the CTP

Two charge-generation elements that are of special interest are the electron gun and the photocathode–MCP assembly. These components perform electron addressing of the CTP and therefore rely on the secondary electron emission characteristics of the target to deposit bipolar charge patterns. The secondary electron emission characteristic of a material is a plot of the ratio $\delta(E_p)$ of the number of secondary electrons (sec. elec.) emitted from the surface to the number of incident primary electrons (pri. elec.) as a function of primary electron energy E_p, that is,

$$\delta(E_p) = \frac{\text{No. sec. elec.}}{\text{No. pri. elec.}}, \tag{4}$$

where

$$E_p = e(V_k - V_s). \tag{5}$$

V_k is the effective cathode voltage and V_s is the effective CTP surface voltage. The secondary electron emission characteristic of a CTP has been measured and the resultant curve is plotted in Fig. 4.

When a CTPSLM is operated below the first crossover point of the characteristic, where $\delta < 1$, the surface of the material will charge negatively because of net electron accumulation. On the other hand, when the device is operated between the first and the second crossover points, where $\delta > 1$, it is possible to charge the surface either positively or negatively. Positive charging is achieved by collecting the secondary electrons with a collector grid placed in close proximity to the CTP, whereas negative charging is achieved by simply permitting the emitted secondary charge to fall back to the surface.

From Fig. 4 we see that, for a bare CTP, δ has a peak value of 1.3 at $E_p = 200$ eV. To increase the effective δ, the CTP may be overcoated with a secondary electron enhancer coating, such as MgO, which will also typically increase the value of E_p at which δ peaks. For electron-beam-addressed devices, increasing the value of E_p, up to a point, increases the sharpness of the electron image deposited on the CTP, and therefore improves the spatial resolution of the device.

C. Charge-Transfer Efficiency and Storage Time

Given the capacitive coupling between the CTP pins, it is clear that there is a loss of charge sensitivity when a CTP is used in an SLM compared with the case for a non-CTP-based SLM. The charge sensitivity may be defined as

$$\gamma = \frac{V_m(\text{with CTP})}{V_m(\text{without CTP})}, \tag{6}$$

where V_m is the longitudinal component of the voltage developed across a pixel of the light-modulating element that is due to a charge q on that pixel. Clearly

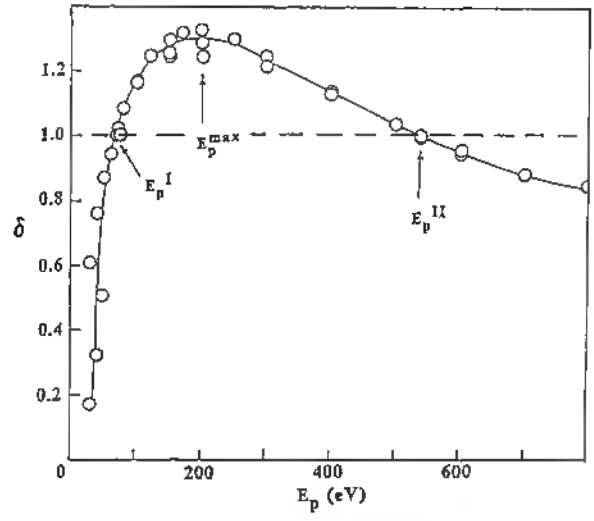

Fig. 4. Measured secondary electron emission characteristic of a CTP.

$\gamma \leq 1$ for all practical cases. Thin CTP's with large interpin separations will optimize the charge-transfer efficiency but at the expense of the spatial resolution.

Long-term (hours) storage of charge by the CTP itself is necessary if CTPSLM's are to exhibit image storage. This means that lateral spreading of the charge from pin to pin must be minimized. Thus the interpin RC value must be maximized. It is therefore necessary that high-resistivity insulating materials be used for the CTP substrate for the case in which long-term storage is required. The typical resistivity of the insulating material used in our CTP's is $\sim 10^{14}\ \Omega$ cm, and charge storage times of the order of 60 s have been observed.

3. Charge-Transfer Plate Membrane-Mirror Light Modulators

Like various types of membrane light modulators given in related works of others,[2–10] charge-transfer-plate membrane-mirror light modulators (CTPMLM's) employ a thin deformable membrane mirror as the light-modulating element. However, the CTPMLM's differ from the previous devices in that the CTPMLM's employ a CTP as the support substrate for the membrane. The characteristics of three types of membrane-mirror devices are discussed: (1) a hardwired matrix-electrode-addressed device in which an array of electrodes is deposited on the addressing side of the CTP and driven by a bank of voltage amplifiers, (2) an optically addressed device (which is photocathode–MCP driven), and (3) an electron-beam-addressed device in which a high-resolution electron gun is used as the charge-generation element. All three of these devices employ the same basic CTP–membrane anode structure as shown in Fig. 5.

A. CTP–Membrane Anode Fabrication

In order to fabricate the CTP–membrane anode assembly, it is necessary first to create the pixel wells into which the membrane mirror deforms when addressed. Two approaches are used: the etched-pin method, and the etched-overcoat method. With the etched-pin method, the pins on one side of the CTP are etched back ~ 3 μm to form shallow wells. The polymeric membrane is then bonded onto the CTP surface that contains the wells such that a reliable bond between the two dielectric surfaces is established by van der Waals forces. The resultant membrane pixels appear in a hexagonal close-packed array that matches that of the CTP conductors. The exposed surface of the membrane is then metallized to convert it to a flexible mirror as well as to provide an electrode to which a potential $V_m(t)$ can be applied during operation. This approach yields one well per pixel.

With the etched-overcoat approach, an insulating layer is first deposited over one face of the CTP and the wells are etched out of the insulating layer. The approach offers tremendous flexibility in the design of the pixel pitch, pixel diameter, and membrane tension. This is because the membrane tension is determined almost exclusively by the materials used for the membrane and the insulating well layer. When photolithographic techniques are used to etch the wells, extremely high spatial uniformity can be achieved, thereby leading to the SLM's with low fixed-pattern noise. Of course, this approach also permits the possibility of oversampling each pixel with several pins, which is important for some applications.

The lifetime of the polymeric membrane was found to be excellent when it was encapsulated in a hermetically sealed vacuum chamber at the readout face of the device. In fact, one of our first membranes to be operated within the hermetically sealed chamber was still functioning normally (with minimal degradation) after more than one year of intermittent use.

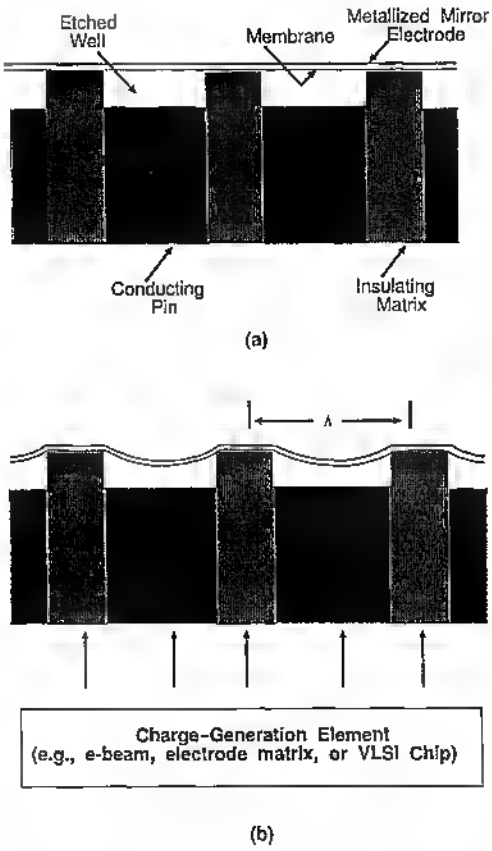

Fig. 5. Deformable membrane mirror stretched over the wells of the CTP: (a) membrane in the unaddressed state, (b) membrane deformation in response to a charge pattern on the CTP.

B. Principles of Operation

The basic operation of the CTPMLM's is such that, in the unaddressed state, the membrane mirror, which is under a slight tension, is flat [see Fig. 5(a)] and all the readout light is reflected into the zero order. In the optically addressed and electron-beam-addressed devices, for example, images are written by depositing a charge pattern $\sigma(x, y)$ on the addressing face of the CTP. This pattern of charge generates electrostatic forces that deform the membrane (in a corresponding pattern) into the underlying wells [see Fig. 5(b)].

Thus the readout light that reflects from the membrane mirror is phase modulated. The amount of deformation increases as the accumulated charge density on the CTP pins increases, leading to gray-scale phase modulation of the readout light. The spatially periodic (hexagonal) phase modulation of the readout wave front causes light to be scattered out of the zero order into higher orders.

The electrostatic force attracting the membrane into a pixel well is easily seen by considering a net charge q deposited onto the corresponding pin. If we assume, for simplicity, that the separation between the membrane and the pin (well depth) is approximately uniform and is much less than the diameter of the pin, the situation resembles that of a parallel plate capacitor, and the force F attracting the membrane to the pin is therefore approximately given by

$$F = qV/2S = \frac{q^2}{2\epsilon_0 A}, \tag{7}$$

where V is the voltage between the membrane and the pin, S is the well depth, A is the area of the well, and ϵ_0 is the permittivity of free space. As charge is added to the pin, the membrane deforms into the well until the restoring force exerted by the tension on the membrane exactly cancels the attractive force.

Altering device parameters such as well diameter a and well depth S has a profound effect on the voltage required to deflect the membrane. It has been shown that the membrane deflection d is given by the equation[5]

$$d = (a^2\epsilon_0 V^2)/(32TS^2), \tag{8}$$

where T is the membrane tension. Thus it is seen that for a voltage-driven device, the operating voltage scales as the ratio of well depth to well diameter $[V \propto (S/a)(Td)^{1/2}]$, whereas for a current-driven device the required charge scales as the well diameter a and is independent of the well depth $[q \propto a(Td)^{1/2}]$. Hence the gray-scale modulation is a nonlinear function of the accumulated CTP surface charge.

When the device is read out with coherent laser light and a classical two-lens spatial filtering system is used to manipulate the light modulated by the membrane, the pattern of light in the Fourier plane of the system also exhibits the hexagonal symmetry of the membrane mirror pixels. By employing a variety of different spatial filters in the Fourier plane, many different operations can be performed. For example, (1) spatially sampled phase-only modulation of the readout light is achieved if no spatial filter is used, and (2) intensity modulation is achieved through the use of simple Fourier-plane filters, such as those shown in Fig. 6. With a low-pass (zero-order) filter [see Fig. 6(a)] a negative of the write image is formed, and with the special high-pass filter of Fig. 6(b) a positive image is formed. The filter in Fig. 6(b) is essentially a zero-order stop combined with a set of bandpass subfilters centered on the signal-carrying diffracted beams. The bandpass filter [Fig. 6(b)] offers the higher contrast ratio in the output image, assuming the membrane remains flat in its OFF state.

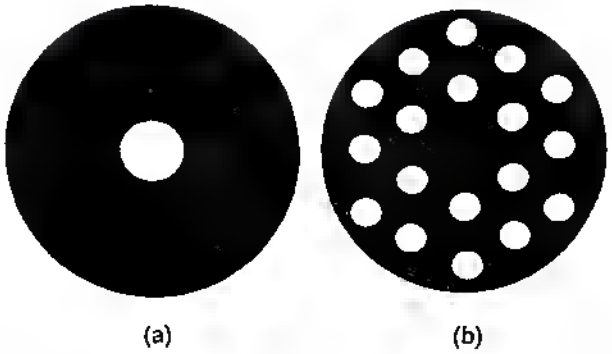

Fig. 6. Amplitude modulation spatial filters: (a) low-pass, zero-order filter; (b) special bandpass Fourier-plane spatial filter.

To gain further insight into the diffraction properties of the membrane, we considered the two-dimensional hexagonal sampling of the membrane mirror and computed the two-dimensional fast Fourier transform of the spatial phase function associated with the deformed mirror. In the model, we assumed a uniform distribution of charge on the CTP, and we assumed that the membrane over each pore is deflected parabolically (a good approximation to the experimentally observed profile). From this exercise, we determined the intensity in the various orders of the diffracted light. Further theoretical and experimental details are given in the paper by Horsky *et al.*[11] in this issue.

C. Hardwired Matrix-Electrode-Addressed CTPMLM

The hardwire-addressed CTPMLM, which is also called the W-MLM for brevity, has the architecture shown in Fig. 7. As can be seen it consists of a CTP–membrane anode assembly with a two-dimensional array of electrodes deposited on the addressing side of the CTP. Each electrode is driven by a separate high-bandwidth, high-current amplifier. An electrode may address either one or several pins, depending on the design and the intended application of the device. Assuming the amplifiers are not current limited, this hardwired device can be driven up to

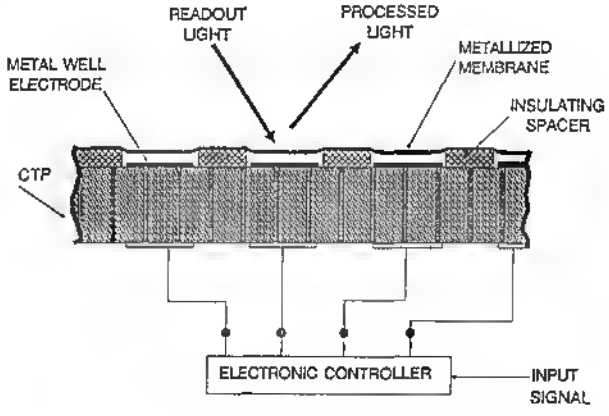

Fig. 7. Architecture of the W-MLM.

the ultimate practical speed of response of the membrane, which is limited by only the first resonant frequency of the membrane (which is estimated to be several megahertz for our devices, based on simple geometric considerations). A 2 × 2 matrix-electrode-addressed MLM was built and a membrane response time on the order of 1 μs was observed, as can be seen in the oscilloscope traces of Fig. 8. Applications of the W-MLM include real-time wave-front phase correction for communication and imaging through turbulence, correction of aberrations in optical instruments, and phase-only Fourier-plane spatial filtering. This device can also function as an array of electrically controlled dynamic focusing mirrors.

D. Optically addressed CTPMLM

One of the optically addressed configurations of the CTPMLM is shown in Fig. 9. This particular configuration is similar to that of the microchannel SLM.[12–14] It is a high-gain, high-sensitivity device that employs the standard CTP–membrane anode, a collector grid, and a photocathode–MCP assembly as the charge-generation element. We also call this device the O-MM for brevity.

In operation, the write-light image incident on the photocathode liberates electrons that are amplified by the MCP's before bombarding the addressing face of the CTP. The purpose of the collector grid is to control the collection of secondary electrons emitted by the CTP surface so that the secondary emission process can be exploited to selectively remove electrons from or deposit electrons onto the CTP, as discussed above. The landing energy of the primary electrons is determined by the effective MCP cathode potential V_k (which tends to be less than ~100 V), the membrane voltage V_m, and the state of charge of the CTP surface.

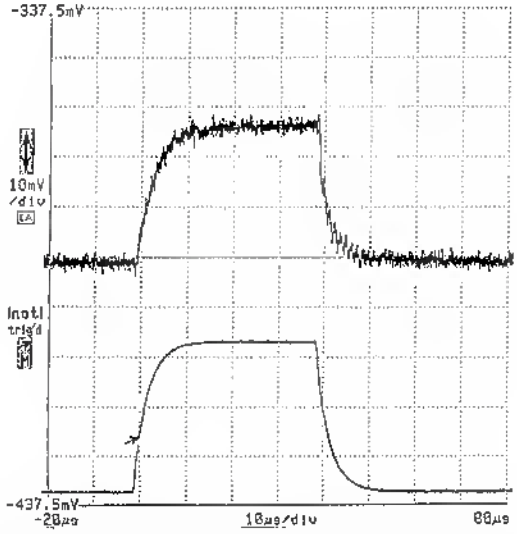

Fig. 8. Optical response (top trace) caused by a voltage step (bottom trace) on one electrode of a W-MLM, indicating a noncurrent-limited membrane response time of ~1 μs. The electrode addressed several pins.

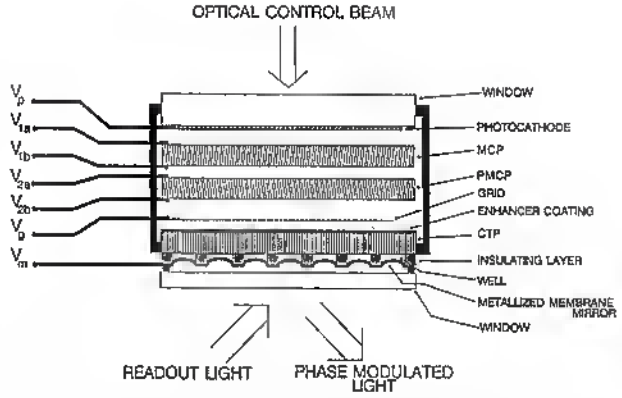

Fig. 9. Structure of the optically addressed photocathode–MCP membrane-mirror light modulator.

In a preliminary vacuum-demountable device that was built without a photocathode and operated with UV write light (the MCP input face acted as an UV photocathode), we demonstrated a spatial resolution of 2 line pairs/mm, and a framing speed of 500 Hz with π radians of phase-modulation depth at 633 nm.

Because of its bipolar charging characteristics and thresholding capability, the O-MLM, like the microchannel SLM, can perform a wide variety of image processing functions. These include image addition, subtraction, and logic operations. Like the W-MLM, applications of the O-MLM include real-time wave-front phase correction for communication and imaging through turbulence, correction of aberrations in optical instruments, phase-only Fourier-plane spatial filtering, and arrays of optically controlled dynamic focusing mirrors.

E. Electron-Beam-Addressed MLM

The structure of the electron-beam-addressed MLM (e-MLM) is illustrated in Fig. 10. It consists of a high-current, high-resolution electron gun, and a CTP/membrane anode assembly. The electron gun converts the control signals from the electronic controller into a charge image that is deposited on the addressing face of the CTP as the electron beam scans the surface. The advantages of electron-beam addressing include essentially wireless operation, and freedom from the fixed-pattern noise that is associated with most other addressing structures. This device offers flickerless gray-scale operation, a high readout light efficiency, a high contrast ratio

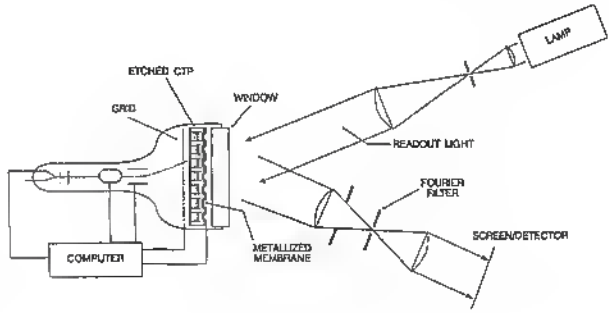

Fig. 10. Structure of the e-MLM.

(>100:1), a potentially large number of pixels (10^6), and readout over a broad wavelength range (UV to long-wave IR).

Applications of the e-MLM are expected to include large-screen projection displays, infrared scene projectors, a computer-generated holographic display, and amplitude and phase-only masks in optical processors. Further details of the e-MLM can be found in the paper by Horsky *et al.*[11] as well as elsewhere.[15,16]

4. Liquid-Crystal CTP Light Modulators

A. E-Beam Liquid Crystal CTPSLM's

The structure of electron-beam liquid-crystal CTPSLM's, which are called e-LCLM's for brevity, is shown in Fig. 11. It consists of an electron gun that scans a focused electron beam across a special CTP–liquid-crystal anode that forms the faceplate of the electron gun. Without some kind of interface component, such as the CTP, electron-beam addressing of a liquid-crystal layer would be impossible. Related e-LCLM's that employ some kind of charge-transfer component are discussed elsewhere.[17–19]

In particular, because CTP's can be polished to an optical flatness of $\lambda/10$ or better, and liquid-crystal alignment layers can be deposited on them by standard techniques, a high-quality liquid-crystal light modulation cell can be readily formed on the CTP by using a glass flat as the second confining surface. Electron-beam-addressed prototypes of both 45°-twist nematic cells for amplitude modulation and parallel aligned nematic cells for phase modulation have been built. The amplitude modulation cells are ~3 μm thick, while very thick cells (~20 μm) were used for the phase modulators.

A novel electron-beam-addressing scheme that exploits the secondary electron emission characteristics of the CTP was employed to ensure that the time-averaged addressing voltage across the CTP was zero. Liquid crystals undergo electrochemical degradation when exposed to long-term dc fields. By writing the appropriate charge distributions on the CTP surface, dynamic lenses of varying focal lengths were demonstrated with the phase-modulating e-LCLM's. Coherent light amplitude image generation with a contrast ratio of 200:1 and a spatial resolution of 3 line pairs/mm was also demonstrated. Further details of work on the above-mentioned e-LCLM's can be found in the paper by Melnik *et al.*[20] and elsewhere.[21,22]

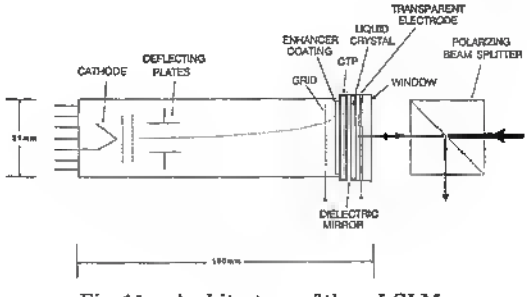

Fig. 11. Architecture of the e-LCLM.

Applications of the phase-only e-LCLM include programmable general-purpose optical elements, nearly real-time computer-generated holographic displays, phase-only spatial filters, wave-front phase correction for communication and imaging through turbulence, and the correction of aberrations in optical instruments. The amplitude device will find applications in projection displays and as an input-plane transducer or Fourier-plane filter in optical processors.

B. Optoelectronic VLSI Liquid-Crystal CTPSLM's

Currently we are investigating both electrically addressed and optically addressed optoelectronic silicon VLSI circuit liquid-crystal CTPSLM's (VLSI LCLM's). These devices have the general structures shown in Fig. 12, in which VLSI chips are bump bonded to CTP–liquid-crystal anode assemblies to form SLM's. The optically addressed devices employ either photodiodes or phototransistors as the charge-generation element. In both devices, extra circuitry added at each pixel along with short-range electrical interpixel communication converts these devices to smart SLM's. Devices that emply both nematic and ferroelectric liquid crystals are being investigated.

The designs shown here have several advantages over the initial approaches pursued by others,[23–30] in which the liquid crystal is in direct contact with the

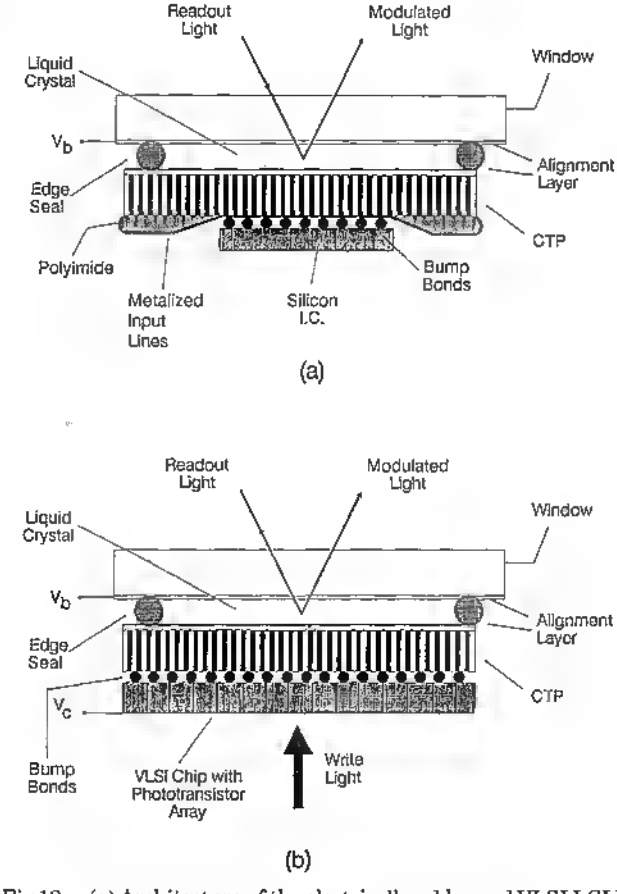

Fig 12. (a) Architecture of the electrically-addressed VLSI LCLM, (b) architecture of the optically addressed VLSI LCLM.

VLSI chip. These initial devices had to be built without an alignment layer on the chip because of possible damage to the chip by alignment layer processing. The specific advantages of using a CTP are (1) no possible damage to the chip from alignment layer deposition and processing, (2) the CTP permits the use of two liquid-crystal alignment layers and so there is no loss of contrast ratio in the CTP-based devices, and (3) excellent spatial uniformity can be achieved in the liquid-crystal cell because the CTP can be polished flat to $\lambda/10$. These devices should be ideal for optical signal processing and computing applications.

5. Summary

CTP's permit the development of a rich class of SLM's. The SLM's that are discussed here include membrane mirrors and liquid crystals, and driving schemes include electron beams, hardwire electrodes, and VLSI chips. Clearly, polymers, oil films, organic and inorganic crystals are also potential light modulation materials that mate well with CTP's. The advantages of using a CTP in a SLM structure include repairability of the SLM in the sense that the light-modulation element may be changed at will without interfering with the charge-generation element, and the versatility of being able to mate any charge-generation element with any light-modulation material. The disadvantages include the loss of charge efficiency because of the added capacitance of the CTP, and a possible loss of spatial resolution if the CTP resolution is not sufficiently high.

The goal of future research in this area is to increase the spatial resolution and decrease the interpin capacitance of the CTP's, as well as to develop large-area ($\sim$100-mm-diameter) CTP's and increase the leak-tightness yield. This will permit the development of low-cost CTPSLM's with millions of pixels that could find applications in areas such as large-screen, high-definition projection displays, infrared scene projectors, and industrial inspection systems.

This paper is an outgrowth of research that spans 1987–1991 that has been sponsored, in part, by the U.S. Air Force under contract F30602-86-C-0209, the U.S. Army Strategic Defense Command under contract DASG60-87-C-0039, the U.S. Naval Research Laboratory under contracts N00014-87-C-2290 and N00014-89-C-2021, the U.S. Army Missile Command under contract DAAH01-89-C-A014, NASA under contract NAS9-18322, and the National Science Foundation under grant ISI-89-61378.

6. References

1. C. Warde and A. D. Fisher, "Spatial light modulators: applications and functional capabilities," in *Optical Signal Processing*, J. Horner, ed. (Academic, New York, 1987), pp. 477–523.
2. K. Preston, Jr., "An array optical spatial phase modulator," in *Proceedings of the International Solid State Circuits Conference* (Institute of Electrical and Electronics Engineers, New York, 1968), p. 100.
3. K. Preston, Jr., *Coherent Optical Computer* (McGraw-Hill, New York, 1972).
4. J. A. van Raalte, "A new schlieren light valve for television projection," Appl. Opt. **9**, 2225–2230 (1970).
5. F. Reizman, "An optical spatial phase modulator array, activated by optical signals," in *Proceedings 1969 Electro-Optical Systems Design Conference*, (Institute of Electrical and Electronics Engineers, New York, 1969), pp. 225–230.
6. L. E. Somers, "The photoemitter membrane light modulator image transducer," in *Advances in Electronics and Electron Physics* (Academic, New York, 1972), Vol. 33A, p. 493.
7. A. D. Fisher, L. C. Ling, J. N. Lee, and R. C. Fukuda, "Photoemitter membrane light modulator," Opt. Eng. **25**, 261–268 (1986).
8. P. B. Rolsma, J. N. Lee, T. K. Oh, and L.-C. Ling, "Experimental parameters of the photoemitter membrane spatial light modulator," Appl. Opt. **28**, 4816–4825 (1989).
9. D. R. Pape, "Optically addressed membrane spatial light modulator," Opt. Eng. **24**, 107–110 (1985).
10. D. R. Pape and L. J. Hornbeck, "Characteristics of the deformable mirror device for optical information processing," Opt. Eng. **22**, 675–681 (1983).
11. T. N. Horsky, C. M. Schiller, G. J. Genetti, T. N. Tsakiris, D. M. O'Mara, R. Jurgilewicz, and S.-D. Lee, and C. Warde, "Electron-beam-addressed membrane mirror light modulator for projection display," Appl. Opt. **31**, 3980–3990 (1992).
12. C. Warde, A. M. Weiss, A. D. Fisher, and J. I. Thackara, "Optical information processing characteristics of the microchannel spatial light modulator," Appl. Opt. **20**, 2066–2074, 1991.
13. C. Warde and J. I. Thackara, "Oblique-cut $LiNbO_3$ microchannel spatial light modulator," Opt. Lett. **7**, 344–346 (1982).
14. C. Warde and J. I. Thackara, "Operating modes of the microchannel spatial light modulator," Opt. Eng. **22**, 295–702 (1983).
15. T. N. Horsky, G. J. Genetti, D. M. O'Mara, C. M. Schiller, and C. Warde, "Electron beam-addressed membrane light modulator," in *Spatial Light Modulators and Their Applications*, Vol. 14 of 1990 OSA Technical Digest Series, (Optical Society of America, Washington, D.C., 1990), pp. 170–173.
16. T. N. Horsky, C. M. Schiller, G. J. Genetti, D. M. O'Mara, W. S. Hamnett, and C. Warde, "Electron-beam addressed membrane light modulator for IR scene projection," in *Infrared Technology XVII*, B. F. Andresen and I. J. Spiro, eds., Proc. Soc. Photo-Opt. Instrum. Eng. **1540**, 527–532 (1991).
17. J.-A. Zhao, S.-S. Tung, and L. Ruan, "A study of liquid crystal light valve for large-screen projection TV," Displ. Technol. **1**, 151–158 (1986).
18. T. S. Buzak, R. S. Vatne, G. A. Nelson, and D. E. Whitlow, "Electron-beam-addressed light valve operating modes and performance," in *1987 SID International Symposium Digest of Technical Papers* (Society for Information Display, Playa Del Rey, Calif., Vol. 1987), pp. 64–67.
19. W. C. Nixon and C. E. Bryan, "Light value," British patent WO85/01362 (28 March 1985).
20. G. A. Melnik, G. C. Gilbreath, T. N. Tsakiris, R. Jurgilewicz, D. M. O'Mara, T. N. Horsky, and C. Warde, "Operating modes of the charge-transfer-plate liquid-crystal phase modulator," Appl. Opt. **31**, 3892–3897 (1992).
21. G. A. Melnik, G. J. Genetti, T. N. Horsky, D. M. O'Mara, T. N. Tsakiris, C. Warde, and C. G. Gilbreath, "Electron beam-addressed liquid crystal phase modulator," in *Spatial Light Modulators and Their Applications*, Vol. 14 of 1990 OSA Technical Digest Series (Optical Society of America, Washington, D.C., 1990), pp. 185–1988.
22. P. W. Hirsch, I. Farber, and C. Warde, "Development of an e-beam charge-transfer liquid crystal light modulator," in *Spatial Light Modulators and Applications*, Vol. 8 of 1988

OSA Technical Digest Series (Optical Society of America, Washington, D.C., 1988), pp. 11–14.
23. D. A. Jared and K. M. Johnson, "Optically addressed thresholding very-large-scale-integration/liquid-crystal spatial light modulators," Opt. Lett. **16,** 967–969 (1991).
24. D. A. Jared, R. Turner, and K. M. Johnson, "Electrically-addressed spatial light modulator that uses a dynamic memory," Opt. Lett. **16,** 1765–1767 (1991).
25. T. J. Drabik and M. A. Handshy, "Silicon VLSI/ferroelectric liquid crystal technology for micropower optoelectronic computing devices," Appl. Opt. **29,**5220–5225 (1990).
26. M. A. Handshy, T. J. Drabik, L. K. Cotter, and S. D. Gaalema, "Fast ferroelectric-liquid-crystal spatial light modulator with silicon-integrated-circuit active backplane," in *Optical and Digital Gallium Arsenide Technologies for Signal Processing Applications,* (M. P. Bendett, D. H. Butler, A. Prabhakar, and A. Yang, eds., Proc. Soc. Photo-Opt. Instrum. Eng. **1291,** 158–164 (1990).
27. L. K. Cotter, T. J. Drabik, R. J. Dillon, and M. A. Handshy, "Ferroelectric-liquid-crystal/silicon-integrated-circuit spatial light modulator," Opt. Lett. **15,** 291–293 (1990).
28. D. J. McKnight, D. G. Vass, and R. M. Sillitto, "Development of a spatial light modulator—a randomly addressed liquid crystal over MOS array," Appl. Opt. **28,** 4757–4762 (1989).
29. I. Underwood, D. G. Vass, and R. M. Sillitto, "Evaluation of an nMOS VLSI array for an adaptive liquid-crystal spatial light modulator," Proc. Inst. Electr. Eng. **133,** 77 (1986).
30. W. A. Crossland, M. J. Birch, D. G. Vass, I. Underwood, S. A. Reid, and S. G. Latham, "Silicon active backplane spatial light modulators using ferroelectric liquid crystals," in *Spatial Light Modulators and Their Applications,* Vol. 14 of 1990 OSA Technical Digest Series (Optical Society of America, Washington D.C., 1990), pp. 94–97.